Annals of Nuclear Energy 167 (2022) 108792

Contents lists available at ScienceDirect

Annals of Nuclear Energy

journal homepage: www.elsevier.com/locate/anucene

Aerosol generation from graphite at high temperature: Role of heating rate and air flow rate

S.K. Yadav [c,*], Manish Joshi [b], P. Shukla [a], Arshad Khan [b]

[a] Department of Mechanical Engineering, Indian Institute of Technology (BHU), Varanasi, India
[b] Radiological Physics and Advisory Division, Bhabha Atomic Research Center, Mumbai, India
[c] Department of Mechanical Engineering, Institute of Engineering Technology, Lucknow, India

ARTICLE INFO

Article history:
Received 18 December 2019
Received in revised form 10 August 2021
Accepted 23 October 2021
Available online 23 November 2021

Keywords:
Aerosol particles
Graphite
HTR
Oxidation

ABSTRACT

Behavior of graphite at high temperature in terms of emission characteristics of aerosols has received notable importance in the recent past. Information on the physico-chemical characteristics of generated particles during air ingress conditions for high temperature reactors (HTRs) is crucial for design and safety considerations. The present study focuses on studying the effects of varying heating rate and air flow rate on the number concentration characteristics of particles and gases (CO and CO_2) generated from heated graphite. Overall, the peak of evolution profile of number concentration of particles and volume concentration of CO gas was observed in between 600 and 800 °C. With an increase in heating rate, higher particle number concentration and shifting of peak towards high temperatures was noted. Although this trend remained more or less similar, number concentration reduced with the increase in air flow rate. Experimental observations have also been supplemented with plausible mechanism in this work.

1. Introduction

Pollution contributed by power generation sources poses a serious threat to health and environment (World Health Organization, 2019). Power generation with reduced emission of polluting gases and combustion products is a challenging technological task (Akhmat et al., 2014). Nuclear power plants play a futuristic role in meeting the energy demands of our society (Adamantiades and Kessides, 2009). They generate an insignificant amount of greenhouse gases or pollutants during their operation, resulting in small life-cycle environmental burden (Switkowski, 2016; Switkowski, 2007). Different types of nuclear reactors viz. Boiling Water Reactor (BWR), Pressurized Water Reactor (PWR), Pressurized Heavy-Water Reactor (PHWR), Gas- Cooled Reactor (GCR) etc. have been in operation since decades. In comparison to conventional reactor technology, HTRs offer an exciting choice due to their relatively higher conversion efficiency. Starting since early 1960s, High-Temperature Gas-cooled Reactors (HTGRs) have been operated successfully throughout the world (Crossland, 2012; Fütterer et al., 2014). HTR based research in the context of Indian nuclear energy program has also been linked to process heat generation for hydrogen production (Dulera et al., 2017; Dulera and Sinha, 2008).

Graphite is used as structural component (moderator, reflector and fuel block/tube) in HTRs on account of its favorable properties like high strength, high thermal conductivity, low thermal expansion coefficient and low neutron absorption at high temperature conditions (Dulera et al., 2017; IAEA, 2005). Ingress of air into the primary circuit affecting the graphite performance has been postulated as a critical safety issue for both prismatic and pebble bed design type HTRs (Carlson and Ball, 2016). This may occur as a result of failure of the coolant pump triggering a loss of coolant accident (LOCA). The temperature of the fuel rods in such conditions increases significantly resulting in core melting and air ingression (Englert et al., 2017; Ferng and Chi, 2012; Hózer et al., 2003; Steinbrück et al., 2006). Several factors like oxidation, abrasion, coolant erosion, spalling and flaking, carbonization etc. contribute towards the generation of particles/dust in such conditions (Peng et al., 2016; Xu et al., 2017). Oxidation of graphite and the loss of mechanical strength in prismatic type HTRs have been studied in detail as being part of probabalisic safety studies for such reactors. The generated particles in such conditions may have a significant fraction in fine and ultrafine size ranges. Due to their proximity to the fuel/fuel structure and favorable surface properties (e.g. porosity), these particles also provide a surface for adhesion of radioactivity (Sun et al., 2020). The metallic fission

* Corresponding author at: Department of Mechanical Engineering, Institute of Engineering Technology, Lucknow 226021, India.

https://doi.org/10.1016/j.anucene.2021.108792
0306-4549/

products, in particular Cs and Sr, interact strongly with graphite and may get released to the containment and subsequently to the environment in the worst case scenario (Katscher et al., 1990). As these small-sized particles have a large residence time, they have the capability to spread radioactivity from the accident site to far distances and for significant time scales (Chen et al., 2017; Huang et al., 2014; Moormann, 2011). The nuclear reactor research encompassing the impacts of severe accidents in Chernobyl and Fukushima suggested the need of improved designs and advanced safety systems for gaining better public acceptance (Adamantiades and Kessides, 2009; Beresford et al., 2019; Moormann, 2011).

Several studies conducted in past focused on understanding the oxidation behavior of graphite in context of HTRs (Kane et al., 2013; Lee et al., 2014; Luo and Jean-Charles, 2012; Ong, 1964; Schweitzer, 1962). Oxidation of graphite is controlled by chemical kinetics and in-pore diffusion at lower and higher temperature regime, respectively (El-Genk and Tournier, 2011; Kane et al., 2017; Maahs, 1971; Propp, 1998). The transition from one regime to the other has been shown to occur between 600 and 900 °C (Hu et al., 2014; Xiaowei et al., 2004) depending on the microstructure of graphite including its density and impurity levels. Oxidation behavior of graphite depends on its surfaces characteristics (e.g. porosity, corrosion resistance, hardness etc.), reaction controlling parameters (e.g. surface temperature, flow rate, chemical kinetics etc.) and external conditions (e.g. heat equilibrium in the reactor, environmental parameters etc.) (Chi and Chan Kim, 2017; Contescu et al., 2012; Lee et al., 2018; Moormann, 2011). Few studies have also been conducted in order to study the formation and evolution characteristics of graphite particles/dust generated when graphite is exposed to air at high temperature. For pebble bed HTR, dust generation was shown to depend on the air velocity only above the working temperature of 650 °C (Kugeler et al., 1992). In another study with relevance to prismatic type reactors, number and mass characteristics of graphite particles generated on exposing graphite to varying high temperature conditions were measured and interpreted (Yadav et al., 2019a). Number concentration of particles and CO emission was found to be highest at around 700 °C for the graphite specimens used in their work. Although substantial knowledge on the phenomenological aspect of graphite oxidation exists, not much information is available on the mechanism of aerosol generation, its evolution characteristics and the reaction controlling parameters. Heating rate and air flow rate could be two important influencing parameters for in such context. The present work focuses on studying the number concentration characteristics of particles generated by graphite sample exposed to high temperature at varying heating rate and air flow rate conditions. The experiments have been performed in a High Temperature Aerosol facility at the working temperature range of 500–900C. Measurements of number concentration/size distribution of particles and volume concentration of CO and CO_2 gas have been interpreted for gaining theoretical insights.

2. Experimental setup

Experiments in the present work have been carried out in a high temperature aerosol generation and sampling facility. Fig. 1 shows the block diagram for the facility and the experimental arrangements. The facility comprises of a tubular spilt furnace in which the graphite samples were kept and exposed to test conditions. A particle-free air acting as an oxidiser for the heated graphite was supplied to it from one end with the help of an air compressor and filtering arrangement. The air (also acting as the carrier) flow rate was maintained by a rotameter coupled to the air compressor. The outlet of the furnace was designed and equipped to measure the concentration of emitted (if any) particles and gases. An *iso*-kinetic sampling probe was used to ensure representative sample for the generated particles. A double pipe heat-exchanger was used downstream of the isokinetic sampling probe to reduce the temperature of the air from 150 °C at the inlet to less than 40C (working threshold for aerosol instrumentation) at the exit. The aerosol stream coming out from the heat exchanger was also passed through an aerosol diluter for keeping the number concentration within the measurement range of the instruments. The aerosol instrument used in these experiments comprised of a Scanning Mobility Particle Sizer (Nanoscan SMPS3910, Make- TSI, USA) and an Optical Particle Sizer (OPS 3330, Make- TSI, USA). SMPS works on the principle of segregation of particles on the basis of their electrical mobility and frequently used for the measurements in fine and ultrafine particle size ranges (size range of SMPS model used in this work: 10 nm − 420 nm). The working of OPC is based on the scattering of light by particles and its size-range gets limited due to weak intensity patterns of smaller size particles (size range of OPS model used in this work: 300 nm–10 μm). The selection of these models covered the particle size range from 10 nm to 10 μm. These sizers were calibrated with respect to certified latex particle size in separate laboratory test. A gas analyzer (Digas444, Make-AVL, India) was used for the measurement of CO and CO_2 gas concentration during these experiments. More details on the facility, experimental set-up and experimental methodology have been provided in Yadav et al. (2019b).

3. Material and methodology

The test material used in this work was high-density isotropic graphite with 99.96% carbon content by weight. Specimens of dimension 25 mm × 25 mm × 5 mm and weight ≈7 g were used during these experiments. Table 1 specifies the important properties of the graphite sample used in this work (Kumar et al., 2016). Apart from the equivalent boron concentration (which should be lesser than 10 ppm), other properties of the specimens conform to the requirements for 'nuclear grade graphite' (ASTM, 2018). In terms of aerosol emission inventory, the sample grade used in these experiments is expected to be similar to the nuclear grade. A specialized in-house graphite cutting facility was utilized to prepare the specimens used in this work. Two specimens were used in each set of experiment of the test matrix. These samples were cleaned with liquid nitrogen and dried before each experimental run in order to eradicate impurities. A representative picture of the graphite specimen is shown in Fig. 2. Two crucial parameters in terms of scaling the laboratory level experiments to field conditions in the context of this work are 'mechanism of aerosol generation' and 'concentration'. The extreme temperature conditions within the core during severe accidents vaporize the components which then nucleating subsequently. In this scenario, the particles are formed and evolved in ultrafine size ranges (diameter lesser than 100 nm) in the initial stage of accident progression. Graphite exposure to high temperature fulfils this requirement and the concentration of the generated particles occurs with high concentration. In ingress scenario, oxidation of graphite depends on the amount of oxygen and the core heat balance. Experiments with air as the ingress medium simulate the worst case scenario for HTRs where air dominates other coolant gases

3.1. XRD analysis of graphite

X-Ray Diffraction (XRD) analysis of graphite samples in pre-heated condition was carried out by employing Rigaku Miniflex 600 Desktop X-Ray Diffraction System (Rigaku Corporation, Japan), coupled with a HyPix-400MF2D hybrid pixel array detector (HPAD)

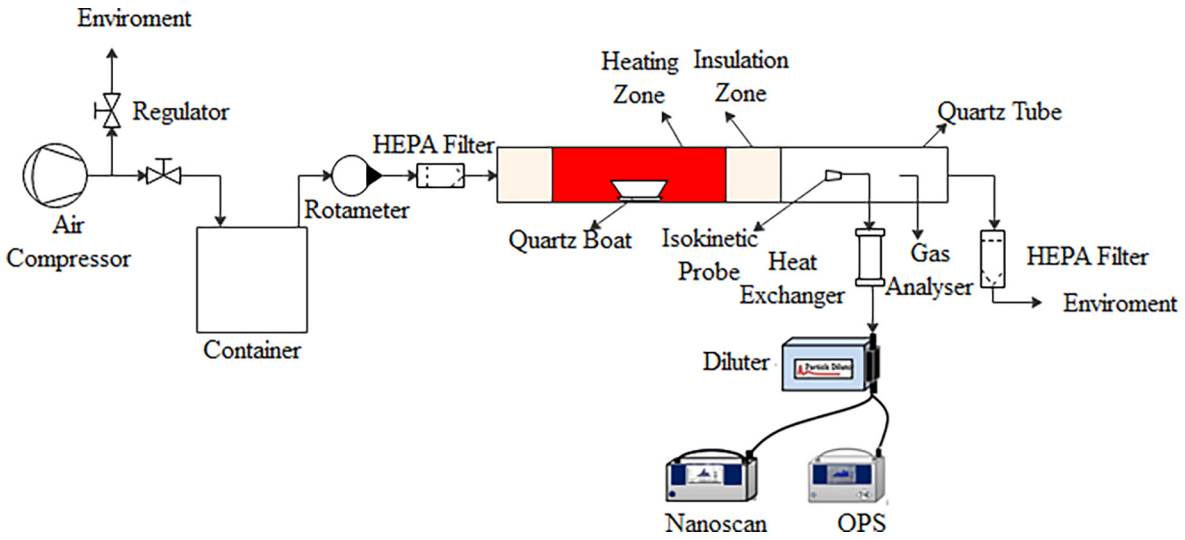

Fig. 1. Schematic diagram of the experimental setup.

Table 1
Properties of graphite specimen.

Properties	Value/Details
Equivalent Boron content	≈13 ppm
Porosity	10.53%
Density	1.82 g cm^{-3}
Compressive strength	113 MPa
Tensile strength	33 MPa
Flexural strength	40 MPa
Thermal conductivity	93 W/mK

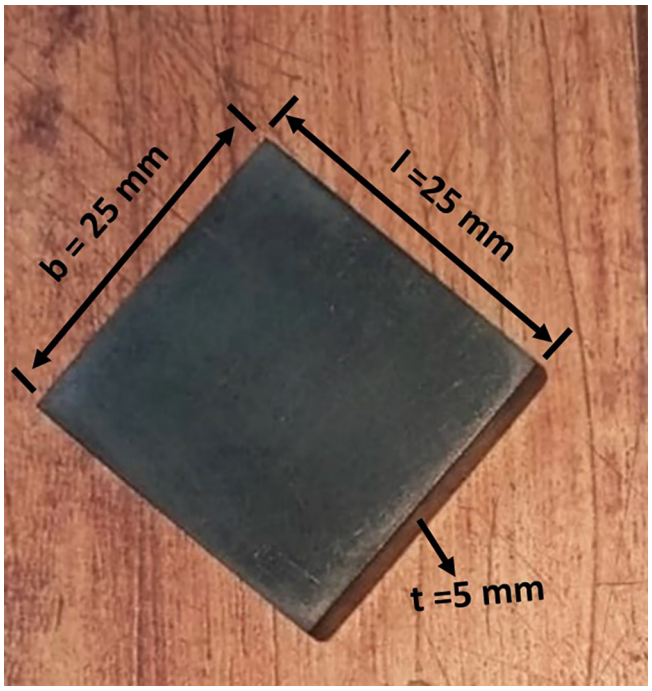

Fig. 2. Picture of graphite sample.

and a 600 W X-ray source. The XRD pattern of graphite sample is depicted in Fig. 3 where the intensity of X-ray diffraction has been plotted with position of sample scanning at 2θ angles. The pattern was found to be matching with standard graphite diffraction pattern (JCPDS card number: 08-0415). Four major peaks corresponding to the crystal planes (002), (101), (004), and (110) can be seen in this pattern. The dominant peak i.e. (002) was sharp, indicating the crystalline structure with an interlayer spacing of 0.346 nm.

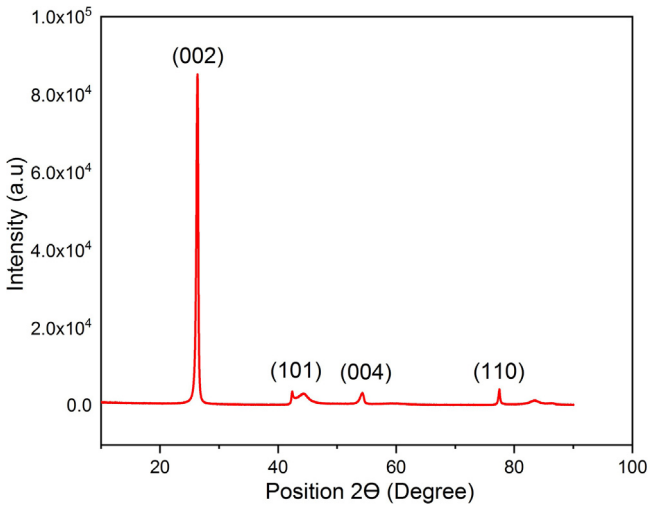

Fig. 3. XRD pattern of graphite sample in pre-heated condition.

3.2. Experimental methodology

As these experiments targeted number concentration of evolution profile of of particles from the exposed samples, background number concentration from the furnace cell was controlled and monitored. As a first step, a high-flow air jet was used to clean the furnace tube and the specimen boat. Aerosol particle sizers and gas analyser were switched on and warmed up for at least 30 min before the actual measurement cycle started. Background aerosol number concentration was measured after starting the nominal airflow. We consider $10^3 cm^{-3}$ as the threshold number concentration for this routine exercise. If the number concentration was found to be more than this value, the set-up was cleaned and checked again. After ensuring that the background number concentration was well below the threshold value, the furnace was operated as per the set protocols. The test specimens placed in the specimen boat were then inserted into the furnace and the

heating cycle was executed. At the end of the experiment, once the furnace temperature reduced to ambient levels residual specimens were taken out for further analysis. As per the objective of the study, furnace was heated at four different heating rates (Fig. 4) during these experiments. The maximum set temperature of 900 °C was attained with heating rates of 2 °C min^{-1}, 4 °C min^{-1}, 6 °C min^{-1} and 8 °C min^{-1}, at four different air flow rates viz. 10, 15, 20 and 25 $Lmin^{-1}$. This limit of temperature was used as being 100 °C higher than the usual transition temperature range of 600–800 °C for the oxidation of graphite. Result from SMPS measurement corresponding to each data point of the Fig. 4 was used for further interpretation.

4. Results and discussion

The characteristics of interest in the present context are the 'total number concentration' and 'number size distribution' of generated aerosol particles and the volume concentration of emitted CO and CO_2 gas during the experiments. Two crucial parameters for air ingress conditions are 'graphite heating rate' and 'air/carrier flow rate'. In all these experiments, both Nanoscan and Optical particle sizer were used for number concentration estimations. However, the number concentration in the size range of 0.3 μm −10 μm using the OPS was found to be insignificant in comparison to that measured in the size range of 10 nm − 420 nm using the SMPS. For example, the peak number concentration for the case of 2° C min^{-1} heating rate and 20 $Lmin^{-1}$ air flow rate was measured as 1.23×10^2 cm^{-3} and 1.79×10^6 cm^{-3} in OPS and SMPS, respectively. As we focus on number concentration characteristics, only result of SMPS measurements are presented hence forth. Necessary protocols for accurate SMPS measurements (Joshi et al., 2012; Wiedensohler et al., 2012) have been followed in this work.

4.1. Number concentration of generated particles

Total aerosol number concentration generated by heated graphite specimens as per the test matrix has been plotted in Fig. 5. Each section of this figure represents the profiles for fixed air flow rate and varying heating rate conditions. Each data point of the curve represent the number concentration of particles generated by oxidizing graphite at a particular temperature. Barring few test conditions, the evolution of number concentration was observed to follow unimodal behavior. For all investigated cases, negligible number concentration was observed below the set temperature of ≈575 °C. In addition, the maximum (peak) number concentration was obtained in the range of 600–800 °C. For fixed air flow rate and heating rate, the number concentration of generated particles increased with the furnace temperature, reaching a maximum value and then reducing for higher temperatures. For instance, peak number concentration for a heating rate of 2 °C min^{-1} and air flow rate of 10 $Lmin^{-1}$ was obtained as 3.94×10^6 cm^{-3} at 642 °C. With an increase in heating rate, the value of peak number concentration increased as well. For an air flow rate of 10 $Lmin^{-1}$, peak number concentration was measured as 3.94×10^6 and 5.13×10^6 cm^{-3} for 2 and 8° C min^{-1} heating rate, respectively. Additionally, the temperature corresponding to the peak number concentration shifted to higher temperature values with the increase in heating rate. Number concentration can be seen to be increasing after the peak temperature as well possibly due to the shift of oxidation reaction kinetics from transition regime to boundary layer regime. The number concentration characteristics of generated particles as a function of graphite/oxidation temperature has been discussed previously (Yadav et al., 2019a). The role of heating rate and air flow rate for the same is discussed in a later section. For air flow rate of 10 $Lmin^{-1}$, distinct number concentration profile for highest heating rate i.e. 8 °C min^{-1} can be attributed to continued particle generation above the temperature corresponding to the peak number concentration. Similar behavior can also be seen for higher heating rates for the case of air flow rates of 15 and 20 $Lmin^{-1}$. However, no clear trend could be established when the air flow rate increased to 25 $Lmin^{-1}$. In general, an increase in air flow rate resulted in the decrease of maximum number concentration recorded for the test condition. As an illustration, maximum concentration was measured as 3.94×10^6, 1.70×10^6, 1.65×10^6 and 1.08×10^6 cm^{-3} for 10, 15, 20 and 25 $Lmin^{-1}$, respectively, at a heating rate of 2 °C min^{-1}. For entire test matrix, maximum (5.13×10^6 cm^{-3}) and minimum (1.08×10^6 cm^{-3}) peak number concentration were obtained for the combination '8 °C min^{-1}, 10 $Lmin^{-1}$' and the combination '2 °C min^{-1}, 25 $Lmin^{-1}$',respectively.

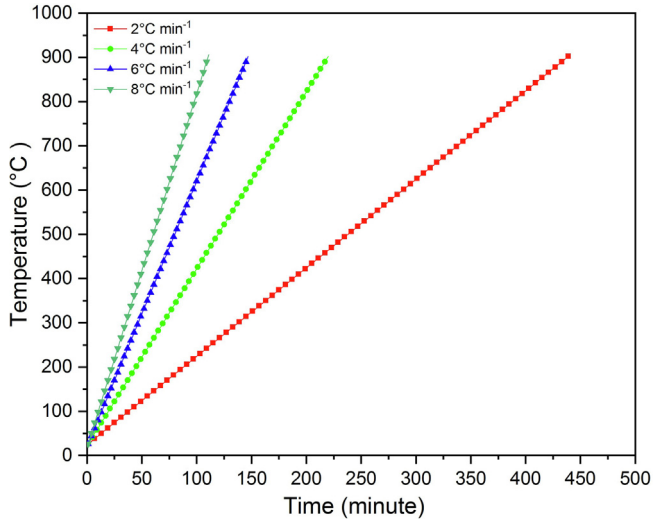

Fig. 4. Temporal profile of furnace heating rate used during experiments.

4.2. Number size distribution of generated particles

Apart from the number concentration, size of aerosol particles is the main characteristic which determines their life and fate (Joshi et al., 2016; Yadav et al., 2019c). Measurement of size distribution for any aerosol spectrum is important and the parameters or the features of the same assist in understanding the process dynamics of the particles. This section discusses the observations of the current work in terms of the number size distribution of the aerosol particles. The size spectrum measured by SMPS (i.e. 10 – 420 nm) during an experimental run was used for discussing these interpretations. Fig. 5(a-d) represent the averaged number size distribution of generated particles from heated graphite specimens at various conditions as per the test matrix. For interpretation purpose, the size spectrum can be divided into 4 parts: 10–50 nm, 50–100 nm, 100–250 nm and 250–365 nm. As evident, the major fraction of particles was measured in the lowest (10–50 nm) and intermediate (100–250 nm) size range. Particle generation in the size range 50–100 nm and 250–365 nm was not observed for the lower heating rates of 2 and 4 °C min^{-1} at all air flow rates. When the heating rate was increased (6 and 8 °C min^{-1}), the number concentration signal in these size ranges was observed for the air flow rates of 10 and 15 $Lmin^{-1}$ (Fig. 6a-b). For still higher airflow rate of 20 $Lmin^{-1}$, no particles were recorded for the size range of 250–365 nm. For the highest air flow rate i.e. 25 $Lmin^{-1}$, no signal was observed in the intermediate size-ranges (Fig. 6d). Similar kind of size distribution inferences were obtained in our earlier work (graphite heating at different temperature) wherein the nucleation

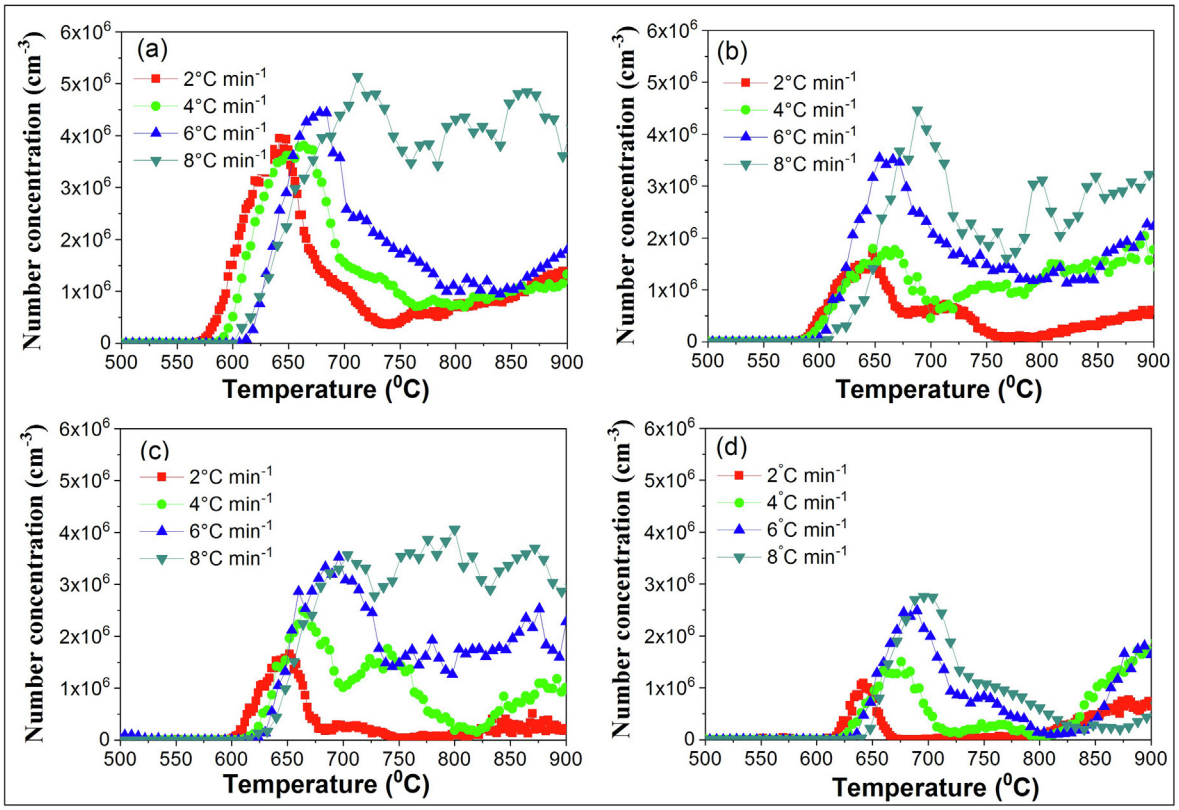

Fig. 5. Total number concentration profile of generated particles at different heating rates and air flow rates of (a) 10 Lmin^{-1} (b) 15 Lmin^{-1} (c) 20 Lmin^{-1} (d) 25 Lmin^{-1}.

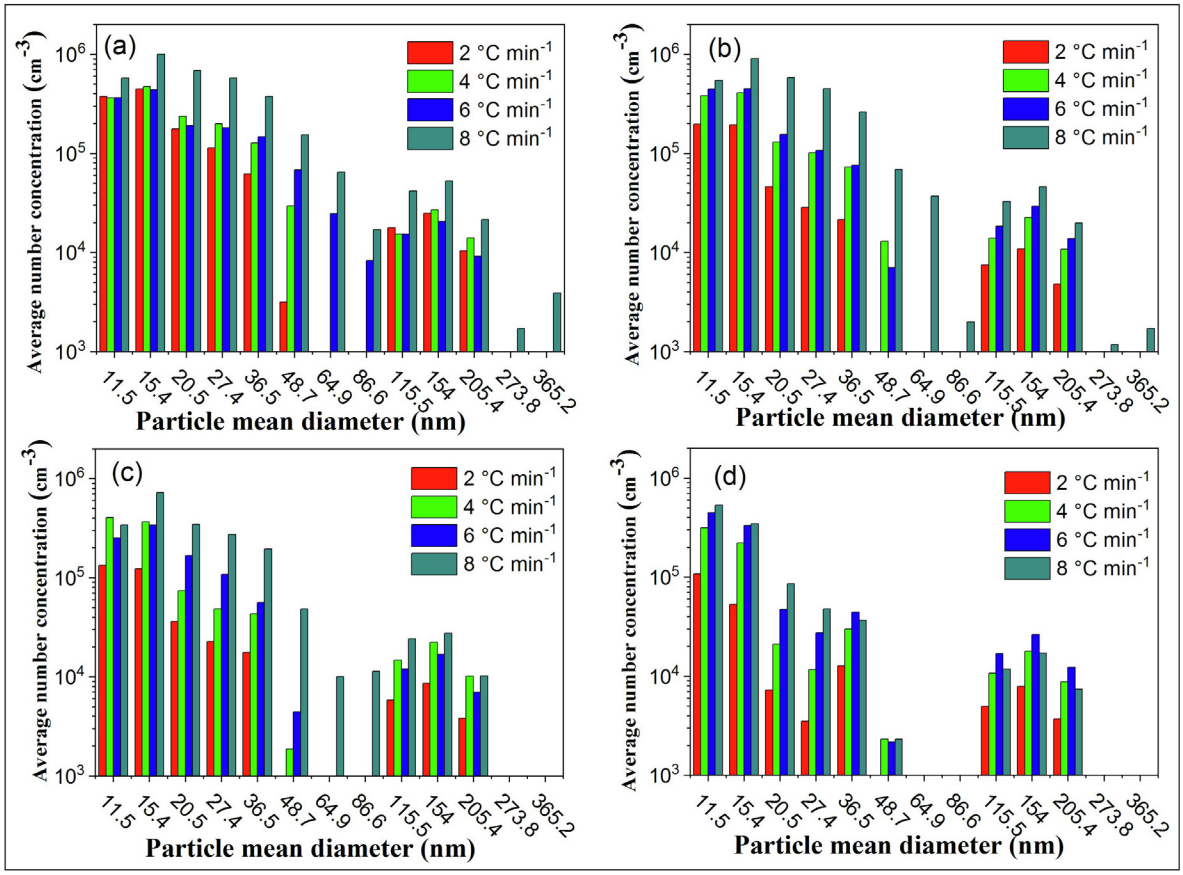

Fig. 6. Particle size distribution at different heating rates and air flow rates of (a) 10 Lmin^{-1} (b) 15 Lmin^{-1} (c) 20 Lmin^{-1} (d) 25Lmin^{-1}.

phenomenon (due to thermal quenching and/or diffusion clustering) and the advective transport of unburnt particles was linked to the observance of number concentration in different size-ranges (Yadav et al., 2019a). Presence of particles in 50–100 nm and 250–365 nm size range at higher heating rate could be due to the size-growth of particles of the nearby regime where the generation is likely to occur. However the decrease in residence time resulted in disappearance of particles in these size regimes leading to a perfect bimodal distribution for the highest flow rate of 25 $Lmin^{-1}$.

4.3. Gas measurement

For the next set of interpretations, emission of CO and CO_2 gases as an effect of oxidation of graphite was studied. Evolution of CO gas concentration for the test matrix has been shown in Fig. 7. No CO concentration was observed below 575 °C for all cases, similar to the behavior for the emission of particles. However, the variation of CO concentration was smooth in comparison to the profile of number concentration of particles. Peak CO concentration was found to be increasing with heating rate for all air flow rate conditions. At 10 $Lmin^{-1}$ (Fig. 7 a), the peak concentration of CO increased from 0.11 v/v % to 0.16 v/v % when the heating rate was increased from 2 to 8 °C min^{-1}. Increasing CO gas concentration indicates the process of incomplete combustion. At higher heating rates, lesser time for completion of combustion reaction leads to a higher CO concentration. It can also be seen from Fig. 7 (a-d) that the concentration level of CO reduced when the air flow rate was increased. An increase in the flow rate enhances the supply of oxygen to the sample, thereby supporting oxidation and hence reducing the concentration of CO. The maximum CO gas concentration of 0.16 v/v% was observed at an air flow rate of 10 $Lmin^{-1}$ (minimum flow rate) and heating rate of 8 °C min^{-1} (maximum heating rate). This observation is also consistent with the levels of particulate concentration presented in Fig. 5a wherein the maximum number concentration was measured at the lowest air flow rate of 10 $Lmin^{-1}$ and the highest heating rate of 8 °C min^{-1}. An increase in incomplete combustion, manifested by an increase in CO gas concentration, increases the particle generation. The shift of peak temperature (temperature corresponding to maximum CO concentration) towards the higher temperature ranges is also consistent when compared to the behavior of number concentration of generated particles.

In addition to CO, the evolution of CO_2 gas concentration was measured for all experiments. As an indicator of complete combustion, its evolution profile should not follow the general trend of CO concentration and the number concentration of particles. The variation of CO_2 gas concentration for entire test matrix has been shown in Fig. 8. The threshold temperature representing the initiation of complete combustion was found to be higher than 575 °C (threshold for particle generation), as expected. For all the cases, CO_2 concentration increased with the increase in temperature attaining saturation above approximately 800 °C. This temperature is above the peak temperature range corresponding to the number concentration profile (Fig. 5a-d). It was also noted that peak concentration of CO_2, similar to CO, shifted to higher temperature with an increase in heating rate. Higher CO2 concentration at lower heating rates indicates the availability of more time for the reaction to proceed towards complete combustion. With the increase in air flow rate, an increase in CO2 concentration is due to enhanced combustion kinetics. Maximum CO_2 concentration (1.5 v/v %) was recorded at highest air flow rate i.e. 25 $Lmin^{-1}$ and lowest heating rate i.e. 2 °Cmin^{-1}.

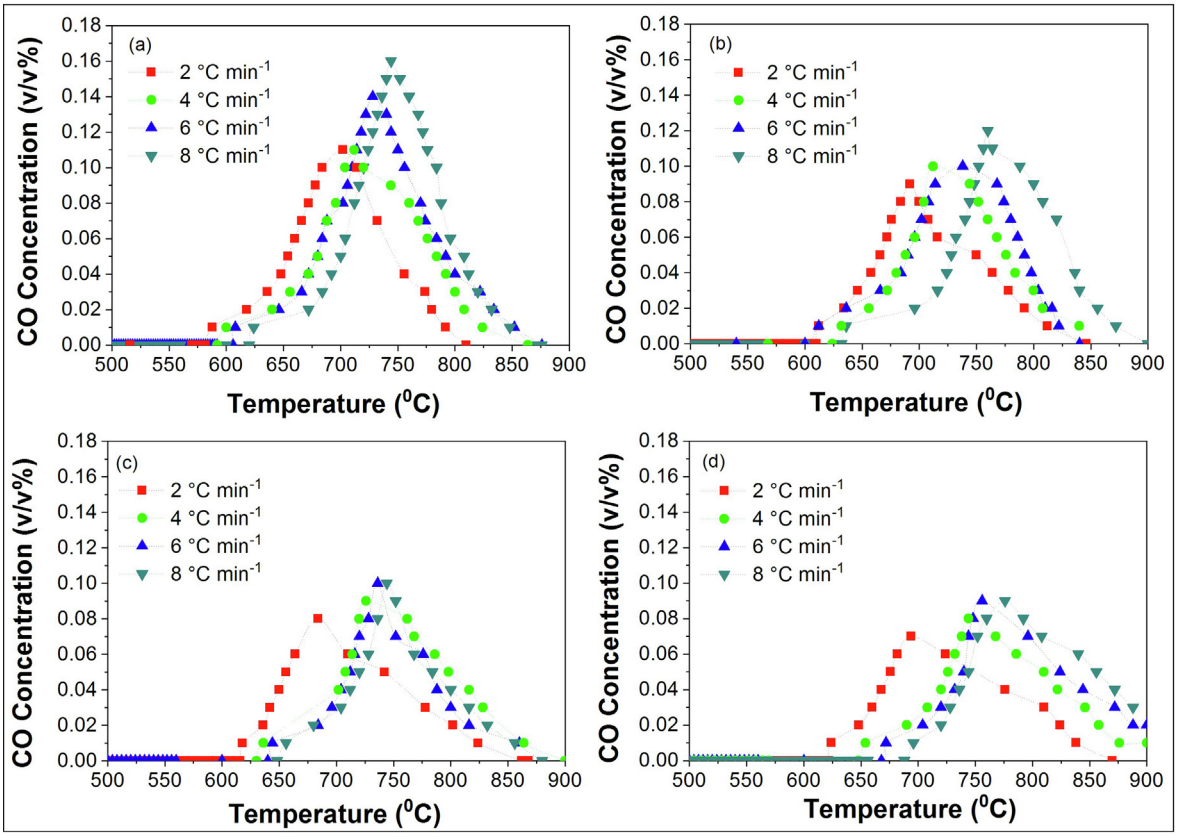

Fig. 7. Carbon monoxide (CO) evolution at different heating rates and air flow rates of (a) 10 $Lmin^{-1}$ (b) 15 $Lmin^{-1}$ (c) 20 $Lmin^{-1}$ (d) 25 $Lmin^{-1}$.

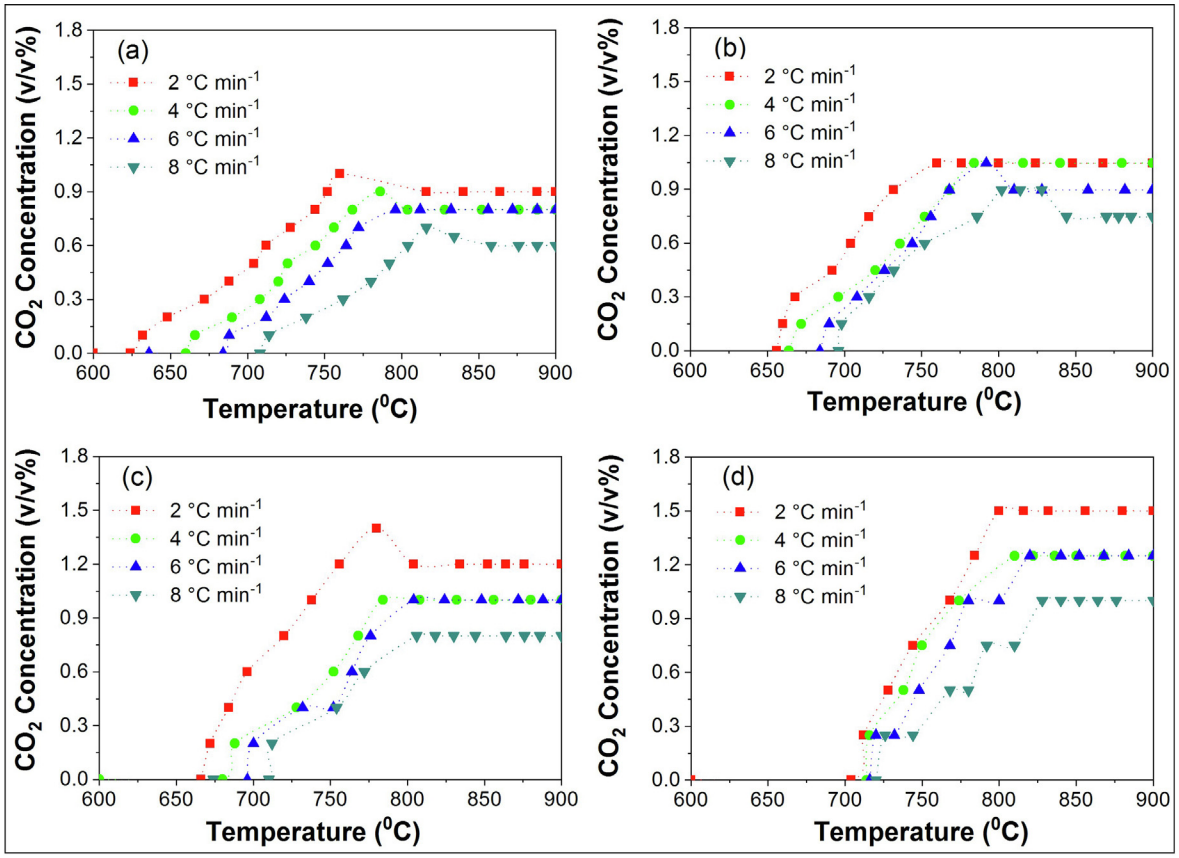

Fig. 8. Carbon dioxide (CO2) evolution at different heating rates and air flow rates of (a) 10 Lmin^{-1} (b) 15 Lmin^{-1} (c) 20 Lmin^{-1} (d) 25 Lmin^{-1}.

4.4. Weight loss analysis

The weight of the residual graphite samples after their exposure to different test conditions was measured and the weight loss was estimated. As a function of temperature (at fixed heating rate and air flow rate), graphite weight loss attributable to conversion to particles and CO is expected to reduce with temperature above transition temperature. In the present work, weight loss of graphite was estimated for varying heating rate and air flow rate conditions (Fig.9). Fig. 9. The weight loss was found to increase with the increase in air flow rate for a fixed heating rate. The increase in air flow increases the combustion resulting in weight loss mostly in terms of emission of CO_2 gas. For a heating rate of 2°-Cmin^{-1}, it increased from 64.68% to 78.97% i.e. a relative increase of 22.09% for 10 and 25 Lmin^{-1}, respectively. The relative increase in weight loss for the same flow rates was measured as 43.23%, 65.14% and 68.27 % for the other heating rates of 4, 6 and 8 °C min^{-1}, respectively. Due to less time for uniform heating and higher incomplete combustion, weight loss reduced with the increase in heating rate. Maximum weight loss percentage of 78.97% was observed at the air flow rate of 25 Lmin^{-1} and heating rate of 2 °Cmin^{-1}.

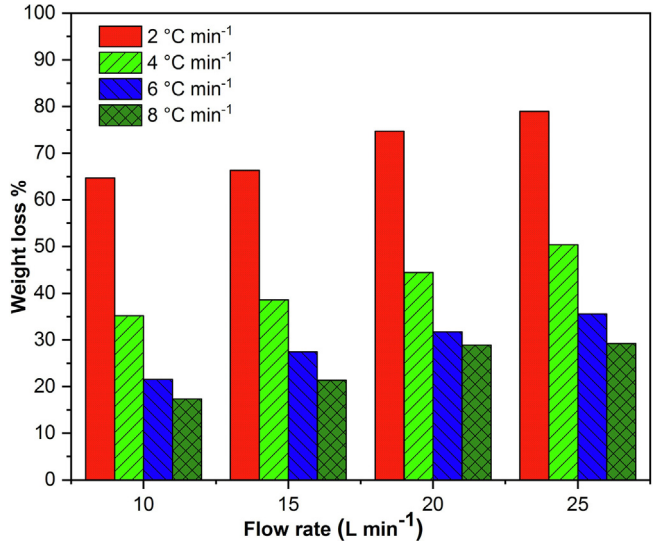

Fig. 9. Weight loss (%) at different heating and air flow rates.

5. Discussion

5.1. Graphite oxidation: Role of temperature

Behavior of graphite under oxidizing conditions can be conceptualized in three regimes- chemical regime, in-pore diffusion regime and boundary layer regime. At extremum temperature regime, progressive model and shrinking core model are adopted for describing solid- fluid reaction (Ahn and Choi, 2017; Rocha et al., 2013). Chemical regime occurs at lower temperature (≈>600 °C for the present study), in which the reaction occurring between graphite and oxidizing gas is very slow and is controlled by the chemical reactivity of graphite and concentration of gas phase oxygen. In this regime, the oxygen penetrates deep into the graphite which gets homogeneously oxidized due to the chemical reaction via its pore system under a rate-limiting step. In this temperature range, the progressive model for solid- fluid reaction

plays a significant role. As per this model, the reactant gas enters and reacts throughout the sample continuously with different rates at different locations. Consequently, the reactant gets converted continuously and progressively throughout the sample (Morin et al., 2017). At the other extreme i.e. above the transition zone (≈ >800 °C for the present study), reactions in graphite take place in the boundary layer. In this domain, the shrinking core model elucidates the phenomenon wherein reactions move from the outer surface to the reacting core surface of the particle releasing combustion products. In such a case, the unreacted core shrinks in size with time during the reaction (Ahn and Choi, 2017; Rocha et al., 2013). For the intermediate temperature range (≈ 600–800 °C), reactions within the graphite particles occur in in-pore diffusion regime. In this regime, the oxidation rate of graphite is controlled by chemical kinetics and oxygen diffusion rate. The transition from progressive model to shrinking core model takes place at transition temperature. A simplistic block diagram of graphite oxidation process has been shown in Fig. 10. More details on the above discussed aspects have been provided elsewhere (Hinssen et al., 1983; Lee et al., 2014, 2013). However it should be noted that the temperature ranges shown in Fig. 10 refers to the general oxidation behavior. The present supplement the available information linking the temperature indices to the generation of particles during the oxidation process.

When graphite samples were oxidised at different heating rates, the peak of the particle concentration and CO was lying mostly in the temperatures range of 600–800 °C (Fig. 5). As discussed above, in this temperature range, oxidation of graphite was controlled by in-pore diffusion regime (transition zone). In this range, the chemical kinetics as well as the diffusion of oxygen into the sample is sufficiently high. This results in incomplete combustion leading to higher CO and particle generation. However, above 800 °C, oxidation is controlled by boundary layer regime. Reactions occur at the surfaces of graphite leading to the decrease in CO and particle concentration. The graphite activation energy also plays a significant role in particle generation. The graphite-oxidation activation energy in air rises to a maximum at about 700 °C, beginning to decrease afterwards. The activation energy is a direct measurement of the thermodynamic energy barrier to the reaction (Kane et al., 2013). It means that around 700 °C, there is highest energy barrier for graphite oxidation and maximum incomplete combustion takes place. This is consistent with the present work as the peak of particle number concentration and CO occurred in the range of 600 to 800 °C. Above 800 °C, oxidation of graphite increases and the reaction proceeds towards complete combustion. A reduction in the sample dimensions and formation of deactivation sites at higher temperatures could also be responsible for lesser particles generation as the combustion process progresses (Radovic et al., 2011).

5.2. Effect of heating rate and air flow rate on particle generation

Generation of particles as an effect of graphite oxidation has been studied in our previous work (Yadav et al., 2019a). The number emission features were linked to the incomplete combustion of the samples. Thermal quenching of hot vapors emitting from the heated zone or the diffusion limited clustering could be the reason of the formation of the particles. These particles then grow by aerosol dynamical processes depending on the source term parameters. Here we discuss the role of heating rate and air flow rate towards the particle generation characteristics. With an increase of heating rate (2 to 8°Cmin^{-1}), number concentration of the particles (Fig. 5) and volume concentration of CO gas (Fig. 7) also increased. For these test conditions, CO_2 emission showed a decreasing trend (Fig. 8). When the heating rate increases, lesser time remains available for the completion of oxidation reaction thus resulting in the generation of higher concentration of incomplete combustion products. Our measurements showed an increase in number concentration of particles in SMPS size range and CO concentration when the heating rate was increased. This also impacts the generation of CO_2 gas in the reverse way i.e. lesser concentration for higher heating rates. On the other hand, an increase in air flow rate enhances the oxygen supply and accelerates oxidation kinetics. The decreased particle as well as CO concentration signifies reaction kinetics tending towards complete combustion in our measurements. It was also observed that the peak of concentration profile (CO, CO_2 and particles) shifted to higher temperature for higher heating rates. Thermal hysteresis could be attributed to this kind of effect seen during the experiments. The temperatures depicted in the evolution profile (Figs. 5, 7 and 8) were recorded by a thermocouple placed in the air stream, just above the sample. As the furnace heating rate increases, thermocouple response changes instantaneously but the sample temperature lags behind. This result in the observance of peaks at the higher temperature as observed in our plots. Thermal hysteresis during pyrolysis of carbonaceous material has been reported in previous studies (Aboulkas and El Harfi, 2009; Niu et al., 2013) as well.

Inferences with respect to the size distribution measurements have been discussed in a previous section. In addition, number concentration in the size range of 10–50 nm was observed to be decreasing with the increase of air flow rate (Fig. 6). For example, number concentration in the SMPS mean size 15.4 nm decreased from 4.45×10^5 cm^{-3} to 5.31×10^4 cm^{-3} at 2 °C min^{-1} heating rate and from 9.97×10^5 cm^{-3} to 3.43×10^5 cm^{-3} at 8 °C min^{-1} heating rate when the air flow rate increased from 10 to 25 Lmin^{-1}. This is

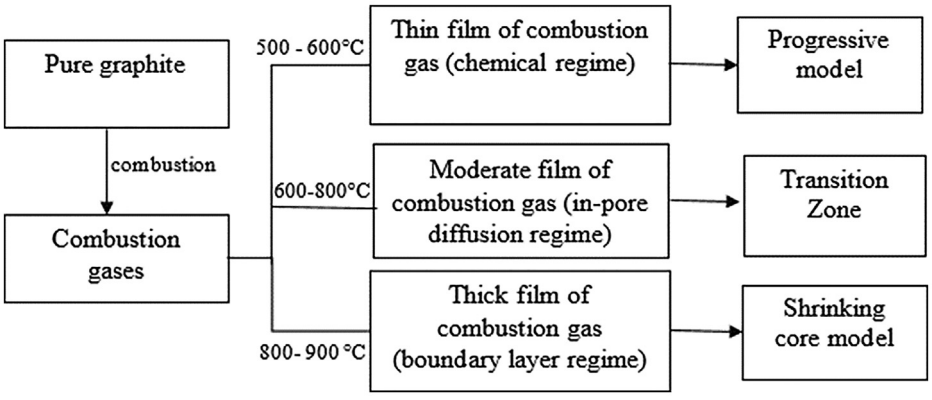

Fig. 10. Graphite oxidation: role of temperature.

again related to the reason as placed above where the increase in air flow rate was linked to effective oxidation of the sample reducing the formation of source term for the nucleation. The observance of particles in 50–100 nm size range and above ≈200 nm for higher heating rates and their disappearance for higher air flow rates are related to the interplay between the growth dynamics and the residence time.

6. Conclusions

This work studied the behavior of high purity graphite in terms of the emission characteristics of particles, CO and CO_2 gases at high temperature and at different heating rate and air flow rates. These experiments were performed in a high temperature aerosol generation and sampling facility. Number concentration measurements mainly focused in the size range ≈10-400 nm while volume concentration was measured for CO and CO_2 gases. Different heating rates i.e. 2, 4, 6 and 8 °C min^{-1} and different air flow rates i.e. 10, 15, 20 and 25 $Lmin^{-1}$ were chosen for defining the test matrix for these experiments. For the entire test matrix, peak concentration of particles and gases was observed in between 600 and 800 °C. Signifying incomplete combustion, maximum concentration of particles and CO was measured as 5.13 × 10^6 cm^{-3} and 0.16 v/v% for heating rate of 8 °$Cmin^{-1}$ and air flow rate of 10 $Lmin^{-1}$ (peak temperature of 712 °C). As expected, concentration of particles and CO gas decreased above the peak (transition) temperature when the temperature of graphite was increased. For these cases, CO_2 evolution profile followed an increasing trend reaching to a saturation value as a result of saturation of the oxidation process. With the increase of heating rate, particle and CO emission was increased due to higher generation of incomplete combustion products (lesser time for complete oxidation). The enhancement of oxygen content at the sample surfaces due to an increase in the air flow rate increases CO2 generation reducing particle generation, simultaneously. Whereas generated particles mostly remained in the size range of 10–50 nm and 100–250 nm, particles in other size channels were also observed for some test conditions. The temperature corresponding to the peak of evolution profiles of particles, CO and CO_2 shifted to higher temperatures with the increase in heating rate. This probably happened due to the lag of the recorded temperature at the thermocouple and the temperature on the sample surface. Graphite heating rate and air flow rate could be two important controlling parameters for air ingress conditions and the results of this work interpret the experimental observations in terms of aerosol emission characteristics for such contexts. Results of this work indicate that the worst combination in terms of oxidation induced particle generation could be the combination of 'high heating rate and low air flow rate' conditions.

CRediT Author Statement

S. K. Yadav: Conceptualization, Data curation, Methodology, analysis Writing – original draft, Writing – review & editing. **P. Shukla:** Formal analysis, Funding acquisition, Investigation, Project administration, Resources, Software, Supervision, Validation, and Visualization. **Manish Joshi:** Conceptualization, Visualization, Writing – review & editing. **Arshad Khan:** Conceptualization, Visualization, Writing – review & editing.

Declaration of Competing Interest

The authors declare that they have no known competing financial interests or personal relationships that could have appeared to influence the work reported in this paper.

Acknowledgment

The authors are grateful for BRNS (Project No. 2013/36/67-BRNS/0577), DAE's financial assistance.

Appendix A. Supplementary data

Supplementary data to this article can be found online at https://doi.org/10.1016/j.anucene.2021.108792.

References

Aboulkas, A., El Harfi, K., 2009. Co-pyrolysis of olive residue with poly(vinyl chloride) using thermogravimetric analysis. J. Therm. Anal. Calorim. 95 (3), 1007–1013. https://doi.org/10.1007/s10973-008-9315-5.
Adamantiades, A., Kessides, I., 2009. Nuclear power for sustainable development: Current status and future prospects. Energy Policy 37 (12), 5149–5166.
Ahn, H., Choi, S., 2017. A comparison of the shrinking core model and the grain model for the iron ore pellet indurator simulation. Comput. Chem. Eng. 97, 13–26. https://doi.org/10.1016/j.compchemeng.2016.11.005.
Akhmat, G., Zaman, K., Shukui, T., Sajjad, F., Khan, M.A., Khan, M.Z., 2014. The challenges of reducing greenhouse gas emissions and air pollution through energy sources: Evidence from a panel of developed countries. Environ. Sci. Pollut. Res. 21 (12), 7425–7435. https://doi.org/10.1007/s11356-014-2693-2.
ASTM, 2018. Graphite Standard Specification for Isotropic and Near-isotropic Nuclear Graphitesi, 1–5. https://doi.org/10.1520/F3114-15.2.
Beresford, N.A., Scott, E.M., Copplestone, D., 2020. Field effects studies in the Chernobyl Exclusion Zone: Lessons to be learnt. J. Environ. Radioact. 211, 105893. https://doi.org/10.1016/j.jenvrad.2019.01.005.
Carlson, D.E., Ball, S.J., 2016. Perspectives on understanding and verifying the safety terrain of modular high temperature gas-cooled reactors. Nucl. Eng. Des. 306, 117–123. https://doi.org/10.1016/j.nucengdes.2016.01.015.
Chen, Z., Chen, X., Zheng, Y., Sun, J., Chen, F., Shi, L., Li, F., Dong, Y., Zhang, Z., 2017. Air ingress analysis of chimney effect in the 200 MWe pebble-bed modular high temperature gas-cooled reactor. Ann. Nucl. Energy 106, 143–153. https://doi.org/10.1016/j.anucene.2017.03.041.
Crossland, I., 2012. In: Nuclear Fuel Cycle Science and Engineering. Elsevier, pp. 3–23. https://doi.org/10.1533/9780857096388.1.3.
Dulera, I.V., Sinha, R.K., 2008. High temperature reactors. J. Nucl. Mater. 383 (1-2), 183–188. https://doi.org/10.1016/j.jnucmat.2008.08.056.
Dulera, I.V., Sinha, R.K., Rama Rao, A., Patel, R.J., 2017. High temperature reactortechnology development in India. Prog. Nucl. Energy 101, 82–99. https://doi.org/10.1016/j.pnucene.2017.04.020.
El-Genk, M.S., Tournier, J.-M., 2011. Development and validation of a model for thechemical kinetics of graphite oxidation. J. Nucl. Mater. 411 (1-3), 193–207. https://doi.org/10.1016/j.jnucmat.2011.01.129.
Englert, M., Frieß, F., Ramana, M.V., 2017. Accident scenarios involving pebble bedhigh temperature reactors. Sci. Glob. Secur. 25 (1), 42–55. https://doi.org/10.1080/08929882.2017.1275320.
Ferng, Y.M., Chi, C.W., 2012. CFD investigating the air ingress accident for a HTGRsimulation of graphite corrosion oxidation. Nucl. Eng. Des. 245, 28–38. https://doi.org/10.1016/j.nucengdes.2012.03.041.
Fütterer, M.A., Fu, L.i., Sink, C., de Groot, S., Pouchon, M., Kim, Y.W., Carré, F., Tachibana, Y., 2014. Status of the very high temperature reactor system. Prog. Nucl. Energy 77, 266–281.
Hinssen, H.K., Katscher, W., Moormann, R., 1983. Kinetics of the graphite/oxygen reaction in the in-pore diffusion controlled regime. Pt. 1 (Juel–1875). Germany.
Hózer, Z., Windberg, P., Nagy, I., Maróti, L., Matus, L., Horváth, M., Csordás, A.P., Balaskó, M., Czitrovszky, A., Jani, P., 2003. Interaction of failed fuel rods under air ingress conditions. Nucl. Technol. 141, 244–256. https://doi.org/10.13182/NT03-A3365.
Hu, Z., Li, Z., Chen, D., Miao, W., Zhang, Z., 2014. CO_2 corrosion of IG-110 nuclear graphite studied by gas chromatography. J. Nucl. Sci. Technol. 51 (4), 487–492. https://doi.org/10.1080/00223131.2013.877407.
Huang, W.H., Tsai, S.C., Chiu, I.C., Chen, C.H., Kai, J.J., 2014. The oxidation effects of nuclear graphite during air-ingress accidents in HTGR. Nucl. Eng. Des. 271, 270–274. https://doi.org/10.1016/j.nucengdes.2013.11.047.
Joshi, M., Khan, A., Anand, S., Sapra, B.K., 2016. Size evolution of ultrafine particles: Differential signatures of normal and episodic events. Environ. Pollut. 208, 354–360. https://doi.org/10.1016/j.envpol.2015.10.001.
Joshi, M., Sapra, B.K., Khan, A., Tripathi, S.N., Shamjad, P.M., Gupta, T., Mayya, Y.S., 2012. Harmonisation of nanoparticle concentration measurements using GRIMM and TSI scanning mobility particle sizers. J. Nanoparticle Res. 14, 1–14. https://doi.org/10.1007/s11051-012-1268-8.
Kane, J.J., Contescu, C.I., Smith, R.E., Strydom, G., Windes, W.E., 2017. Understanding the reaction of nuclear graphite with molecular oxygen: Kinetics, transport, and structural evolution. J. Nucl. Mater. 493, 343–367. https://doi.org/10.1016/j.jnucmat.2017.06.001.
Kane, J.J., Karthik, C., Ubic, R., Windes, W.E., Butt, D.P., 2013. An oxygen transfer model for high purity graphite oxidation. Carbon N. Y. 59, 49–64. https://doi.org/10.1016/j.carbon.2013.02.053.

Katscher, W., Moormann, R., Verfondern, K., Decken, C.B.v.d., Iniotakis, N., Hilpert, K., Christ, A., Lohnert, G., Wawrzik, U., 1990. Fission product behaviour and graphite corrosion under accident conditions in the HTR. Nucl. Eng. Des. 121 (2), 219–225.

Kugeler, K., Epping, C., Schmidtlein, P., Schreiner, P., 1992. Aerosol formation by graphite corrosion in case of water and air ingress to the core of a High-Temperature Reactor. Nucl. Eng. Des. 137 (2), 213–219. https://doi.org/10.1016/0029-5493(92)90020-V.

Kumar, S.A., Venkatesh, K., Swain, K.K., Manisha, V., Kamble, G.S., Pandey, S.P., Remya Devi, P.S., Ghosh, M., Verma, R., 2016. Preparation of in-House graphite Reference Material for Boron.https://inis.iaea.org/search/search.aspx?orig_q=RN:47104468

Lee, J.J., Ghosh, T.K., Loyalka, S.K., 2014. Oxidation rate of graphitic matrix material in the kinetic regime for VHTR air ingress accident scenarios. J. Nucl. Mater. 451 (1-3), 48–54. https://doi.org/10.1016/j.jnucmat.2014.03.033.

Lee, J.J., Ghosh, T.K., Loyalka, S.K., 2013. Oxidation rate of nuclear-grade graphite NBG-18 in the kinetic regime for VHTR air ingress accident scenarios. J. Nucl. Mater. 438 (1-3), 77–87.

Luo, X., Jean-Charles, R., 2012. Research of Oxidation Properties of Graphite Used in HTR-10.

Maahs, H.G., 1971. Oxidation of Carbon At High Temperatures : Reaction-Rate Control or Transport Control. National Aeronautics and Space Administration.

Moormann, R., 2011. Phenomenology of graphite burning in air ingress accidents of HTRs. Sci. Technol. Nucl. Install. 2011, 1–13. https://doi.org/10.1155/2011/589747.

Morin, M., Pécate, S., Masi, E., Hémati, M., 2017. Kinetic study and modelling of char combustion in TGA in isothermal conditions. Fuel 203, 522–536. https://doi.org/10.1016/j.fuel.2017.04.134.

Niu, Y., Tan, H., Liu, Y., Wang, X., Xu, T., 2013. The effect of particle size and heating rate on pyrolysis of waste capsicum stalks biomass. Energy Sources. Part A Recover. Util. Environ. Eff. 35 (17), 1663–1669. https://doi.org/10.1080/15567036.2010.509084.

Ong, J.N.J., 1964. On the kinetics of oxidation of graphite. Carbon N. Y. 2, 281–297. https://doi.org/10.1179/msc.1969.3.1.95.

Peng, L., Zhipeng, C., Yanhua, Z., Jun, S., Fubing, C., Lei, S., Fu, L., Yujie, D., Zuoyi, Z., 2016. Study on air ingress of the 200 MWe pebble-bed modular high temperature gas cooled reactor. Ann. Nucl. Energy 98, 120–131. https://doi.org/10.1016/j.anucene.2016.07.029.

Propp, W.A., 1998. Graphite Oxidation Thermodynamics/Reactions, U.S Department of energy.United States. https://doi.org/10.2172/769038.

Radovic, L.R., Silva-Villalobos, A.F., Silva-Tapia, A.B., Vallejos-Burgos, F., 2011. On the mechanism of nascent site deactivation in graphene. Carbon N. Y. 49 (11), 3471–3487. https://doi.org/10.1016/j.carbon.2011.04.046.

da Rocha, D., Paetzoldb, E., Kanswohl, N., 2013. Chemical Engineering and Processing : Process Intensification The shrinking core model applied on anaerobic digestion. Chem. Eng. Process. Process Intensif. 70, 294–300. https://doi.org/10.1016/j.cep.2013.05.003.

Schweitzer, D.G., 1962. Oxidation and Heat Transfer Studiesin Graphite Channels: I. The Effect of Air Flow Rate on the C-O2 and CO-O2 Reactions. Nucl. Sci. Eng. 12, 59–62. https://doi.org/10.13182/NSE62-A25370.

Steinbrück, M., Miassoedov, A., Schanz, G., Sepold, L., Stegmaier, U., Stuckert, J., 2006. Experiments on air ingress during severe accidents in LWRS. Nucl. Eng. Des. 236, 1709– 1719. https://doi.org/10.1016/j.nucengdes.2006.04.010.

Sun, Q.i., Peng, W., Yu, S., Wang, K., 2020. A review of HTGR graphite dust transport research. Nucl. Eng. Des. 360, 110477. https://doi.org/10.1016/j.nucengdes.2019.110477.

Switkowski, Z., 2016. Climate change and nuclear power. International Atomic Energy Agency, Vienna, Austria.

Switkowski, Z., 2007. Climate change and nuclear power in Australia. Aust. Phys. 44, 90–94.

Wiedensohler, A., Birmili, W., Nowak, A., Sonntag, A., Weinhold, K., Merkel, M., Wehner, B., Tuch, T., Pfeifer, S., Fiebig, M., Fjäraa, A.M., Asmi, E., Sellegri, K., Depuy, R., Venzac, H., Villani, P., Laj, P., Aalto, P., Ogren, J.A., Swietlicki, E., Williams, P., Roldin, P., Quincey, P., Hüglin, C., Fierz-Schmidhauser, R., Gysel, M., Weingartner, E., Riccobono, F., Santos, S., Grüning, C., Faloon, K., Beddows, D., Harrison, R., Monahan, C., Jennings, S.G., O'Dowd, C.D., Marinoni, A., Horn, H.G., Keck, L., Jiang, J., Scheckman, J., McMurry, P.H., Deng, Z., Zhao, C.S., Moerman, M., Henzing, B., De Leeuw, G., Löschau, G., Bastian, S., 2012. Mobility particle size spectrometers: harmonization of technical standards and data structure to facilitate high quality long-term observations of atmospheric particle number size distributions. Atmos. Meas. Tech. 5, 657–685. https://doi.org/10.5194/amt-5-657-2012.

World Health Organization, 2019. Air Pollution and health: Summary. https://doi.org/10.1007/978-94-009-4003-1.

Xiaowei, L., Jean-Charles, R., Suyuan, Y., 2004. Effect of temperature on graphite oxidation behavior. Nucl. Eng. Des. 227 (3), 273–280. https://doi.org/10.1016/j.nucengdes.2003.11.004.

Xu, W., Sun, J., Zheng, Y., Shi, L., 2017. The influence of nuclear graphite oxidation on air ingress accident of HTR-PM. Ann. Nucl. Energy 110, 1242–1248. https://doi.org/10.1016/j.anucene.2017.08.028.

Yadav, S.K., Joshi, M., Sharma, Y., Shukla, P., Kaushik, A., Sapra, B.., Singh, R.., 2019a. Physico-chemical characteristics of graphite aerosols generated during postulated air ingress accident. Ann. Nucl. Energy 132, 100–107.

Yadav, S.K., Khan, A., Shukla, P., 2019b. Development of a high temperature facility for study of aerosol emission behavior of combustible materials. Measurement 139, 308–316. https://doi.org/10.1016/j.measurement.2019.02.067.

Yadav, S.K., Kumar, M., Sharma, Y., Shukla, P., Singh, R.S., Banerjee, T., 2019c. Temporal evolution of submicron particles during extreme fireworks. Environ. Monit. Assess. 191, 1–12. https://doi.org/10.1007/s10661-019-7735-2.